

SCIENTIFIC REPORTS

OPEN

Ptf1a inactivation in adult pancreatic acinar cells causes apoptosis through activation of the endoplasmic reticulum stress pathway

Morito Sakikubo^{1,2}, Kenichiro Furuyama^{1,2}, Masashi Horiguchi^{1,2}, Shinichi Hosokawa^{1,2}, Yoshiaki Aoyama^{1,2}, Kunihiro Tsuboi^{1,2}, Toshihiko Goto^{1,2}, Koji Hirata^{1,2}, Toshihiko Masui^{1,2}, Yuval Dor³, Tomoyuki Fujiyama^{4,5}, Mikio Hoshino⁴, Shinji Uemoto¹ & Yoshiya Kawaguchi²

Pancreas transcription factor 1 subunit alpha (PTF1A) is one of the key regulators in pancreatogenesis. In adults, it transcribes digestive enzymes, but its other functions remain largely unknown. Recent conditional knockout studies using *Ptf1a*^{CreER/floxed} heterozygous mouse models have found PTF1A contributes to the identity maintenance of acinar cells and prevents tumorigenesis caused by the oncogenic gene *Kras*. However, *Ptf1a* heterozygote is known to behave differently from homozygote. To elucidate the effects of *Ptf1a* homozygous loss, we prepared *Elastase-CreERTM; Ptf1a*^{floxed/floxed} mice and found that homozygous *Ptf1a* deletion in adult acinar cells causes severe apoptosis. Electron microscopy revealed endoplasmic reticulum (ER) stress, a known cause of unfolded protein responses (UPR). We confirmed that UPR was upregulated by the activating transcription factor 6 (ATF6) and protein kinase RNA (PKR)-like endoplasmic reticulum kinase (PERK) pathways, but not the inositol requiring enzyme 1 (IRE1) pathway. Furthermore, we detected the expression of CCAAT-enhancer-binding protein (C/EBP) homologous protein (CHOP), a pro-apoptotic factor, indicating the apoptosis was induced through UPR. Our homozygous model helps clarify the role PTF1A has on the homeostasis and pathogenesis of exocrine pancreas in mice.

A great volume of study has identified key transcriptional factors that play central roles in cell specification, growth and differentiation during organogenesis. Even in adult cells, sets of transcriptional factors have been reported to shift cell identity to other cell types. Examples include the Yamanaka factors (*Oct3/4*, *Sox2*, *c-Myc* and *Klf4*) for the creation of iPS cells^{1,2}, the induction of *MyoD* for the direct reprogramming of fibroblasts to myoblasts³, and the induction of *Hnf4α* and one of *Foxa1*, *Foxa2* or *Foxa3* for the transdifferentiation to hepatic cells⁴. These studies demonstrate the dosage of key transcription factors plays an important role in the regulation of cell behavior.

Ptf1a is an indispensable gene for pancreas formation during organogenesis^{5,6}. Using Cre-mediated lineage tracing experiments, we have previously demonstrated that PTF1A functions as a pancreas-fate determinant; the progeny of *Ptf1a*-expressing cells are committed to the pancreatic cell fate, whereas the progeny of *Ptf1a*-deficient cells are committed to the duodenal or bile duct cell fate⁶. While PTF1A is broadly expressed in nascent pancreatic buds, its expression is gradually confined to exocrine lineage during development and finally to acinar cells^{5–8}. Analyses of *Ptf1a* hypomorphic mutant mice revealed that there exists a threshold of the *Ptf1a* mRNA dosage

¹Department of Hepato-Biliary-Pancreatic Surgery and Transplantation, Kyoto University Graduate School of Medicine, Kyoto, Japan. ²Department of Clinical Application, Center for iPS cell Research and Application, Kyoto, Japan. ³Department of Developmental Biology and Cancer Research, The Institute for Medical Research Israel-Canada, Hebrew University-Hadassah Medical School, Jerusalem, Israel. ⁴Department of Biochemistry and Cellular Biology, National Institute of Neuroscience, NCNP, Tokyo, Japan. ⁵International Institute for Integrative Sleep Medicine (WPI-IIS), University of Tsukuba, Tsukuba, Japan. Correspondence and requests for materials should be addressed to Y.K. (email: yoshiyak@cira.kyoto-u.ac.jp)

that allows pancreatic-fate specification and progression along the proper developmental pathway; a reduction of *Ptf1a* mRNA dosage resulted in a decrease in the number of cells that adopt the pancreatic cell fate, a reduction in cell proliferation of early pancreatic precursors, and an impairment of exocrine cytodifferentiation⁹.

Despite accumulating information on PTF1A function and PTF1A dosage during embryonic pancreatogenesis, knowledge on the role of PTF1A in adult pancreas is limited. Originally, PTF1A was found as a transcriptional regulator of digestive enzymes such as amylase and elastase in adult acinar cells⁷. Recently, Krah *et al.* showed that conditional deletion of *Ptf1a* in adult acinar cells resulted in ductal metaplasia and made the cells hypersensitive to *Kras* transformation¹⁰. In addition, Hoang *et al.* reported that *Ptf1a* deletion in adult acinar cells promotes the expression of genes consistent with stomach lineage¹¹. These reports support the notion that PTF1A is required for maintaining acinar cell identity in adults. However, because the studies used *Ptf1a^{CreER/floxed}* compound heterozygote mice, the dosage effect of PTF1A remains unexplored. Considering that adult acinar cells in *Ptf1a* heterozygous mice proliferate more than wild type mice¹² and that oncogenic *Kras*-induced pancreatic cancer progresses more rapidly in *Ptf1a* heterozygous mice¹⁰, the original PTF1A dosage may affect the observations made in these *Ptf1a* conditional knockout studies.

To explore the dosage effects of PTF1A on adult acinar cells, we used *Elastase-CreERTM; Ptf1a^{floxed/floxed}* mice to inactivate PTF1A and tracked the fate of *Ptf1a*-deleted cells by lineage tracing analyses. We found that *Ptf1a* deletion caused not only a shift in identity to duct cells but also severe apoptosis in acinar cells, which resulted in a rapid reduction of pancreatic mass. Furthermore, we found evidence that the changes were associated with ER stress through activation of the PERK-eIF2 α -ATF4 and ATF6 pathways and induction of the pro-apoptotic factor CHOP.

Results

***Ptf1a* conditional knockout caused pancreatic volume loss and acinar apoptosis.** We interbred *Elastase-CreERTM* and *Ptf1a^{floxed}* mice to obtain *Elastase-CreERTM; Ptf1a^{floxed/floxed}* mice (*Ptf1a* cKO mice) and *Elastase-CreERTM; Ptf1a^{+/+}* mice (control) and then crossed them with *Rosa26R* or *Rosa26-RFP* mice for lineage tracing (Supplementary Fig. S1) and injected tamoxifen (0.2 mg/g body weight) at the adult stage. We confirmed the efficiency of PTF1A depletion after Cre-mediated recombination by PTF1A immunostaining. PTF1A positivity per lineage-labeled acinar cells was $74.0 \pm 6.9\%$ in control mice and $4.4 \pm 2.8\%$ in *Ptf1a* cKO mice on day 3, and $84.2 \pm 1.8\%$ in control mice and $1.9 \pm 0.4\%$ in *Ptf1a* cKO mice on day 10, indicating satisfactory depletion of PTF1A in *Ptf1a* cKO mice (Supplementary Fig. S2a,b).

The pancreas of *Ptf1a* cKO mice was significantly edematous on day 10 (Fig. 1a), but had already reduced in size by day 3 (Fig. 1b). To account for the size reduction, we observed acinar-to-ductal metaplasia (ADM) in *Ptf1a* cKO mice^{10,11}. The ADM area was only 2.5% and 1.5% of the whole pancreas on days 3 and 10, respectively, in *Ptf1a* cKO mice (Supplementary Fig. S3). Considering that the ratio of pancreas weight per body weight of *Ptf1a* cKO mice was about two thirds that of control mice (Fig. 1b), ADM alone could not explain the pancreatic size reduction. Indeed, TUNEL staining revealed significantly more cell death by day 3 in *Ptf1a* cKO mice than in control mice, but not on day 10 (Fig. 1c). On the other hand, the number of proliferative (BrdU(+)) cells between control and mutant mice was the same on day 3 and the same on day 10 (Fig. 1c). Thus, accelerated apoptotic cell death by day 3 is presumably the main cause of the pancreatic mass reduction in the mutants.

Consistently, an accelerated cell death of PTF1A-depleted cells was supported by the reduction of lineage-labeled cells in *Ptf1a* cKO mice on day 10 ($43.4 \pm 9.5\%$ in control vs. $6.0 \pm 2.3\%$ in *Ptf1a* cKO mice; see Fig. 2a,b). Interestingly, our lineage tracing analyses revealed non-autonomous cell death in the *Ptf1a*-preserved (X-gal(-)) population of *Ptf1a* cKO mice on day 3 (Fig. 2c). At the same time, a compensatory proliferation of surrounding *Ptf1a*-preserved acinar cells in mutant mice was suggested to have occurred by day 3. As shown in Fig. 2d, we detected BrdU(+) cells in the X-gal(-) population. If the proliferative cells were equally distributed independently of *Ptf1a* deletion, the ratio of X-gal(+) should be equivalent to the ratio of X-gal(+)BrdU(+) cells per total BrdU(+) cells. However, we found the X-gal(+) ratio was higher, suggesting that *Ptf1a*-preserved cells proliferated more than *Ptf1a*-deleted cells in mutant pancreata at this stage. Cell death and proliferation seemed to be balanced on day 3, because the percentage of Cre-recombinase activated (X-gal(+)) acinar cells was unchanged between the two mouse types ($25.3 \pm 5.8\%$ in control and $26.3 \pm 4.7\%$ in *Ptf1a* cKO mice; see Fig. 2a,b). However, compensatory proliferation could not maintain the organ size, and the percentage of X-gal(+) acinar cells was significantly decreased on day 10 (see Figs 1a and 2a,b). Furthermore, the pancreatic volume did not recover by day 20 (Supplementary Fig. S4), which is consistent with a previous report¹¹. The precise mechanism mediating the interaction between *Ptf1a*-deleted and *Ptf1a*-preserved cells warrants future investigation.

Electron microscopy unveiled endoplasmic reticulum stress. To investigate the cell death machinery in *Ptf1a* cKO mice, we performed electron microscopic analyses (Fig. 3). We noticed the emergence of abnormal acinar cells characterized by significantly dilated ER lumen in *Ptf1a* cKO pancreata on day 3 (compare Fig. 3b,d). This characteristic phenotype suggests ER stress was caused by an accumulation of unfolded or misfolded proteins within the ER lumen^{13,14}. The ER lumen size was restored to normal by day 10 in mutant mice (compare Fig. 3e-h).

ATF6 cleavage was higher in *Ptf1a* cKO mice on day 3. Our electron microscopy observations prompted us to analyze the unfolded protein response (UPR) to ER stress including activation of the ATF6, IRE1 and PERK-eIF2 α -ATF4 pathways, which can contribute to apoptosis¹⁵. Western blotting revealed that total ATF6 expression was similar in the two mouse groups on days 3 and 10 (Fig. 4a,b,d,e). However, cleaved ATF6 was more highly expressed in *Ptf1a* cKO mice on day 3 but not on day 10 (Fig. 4a,c,d,f), indicating that the ATF6 pathway was activated on day 3 but deactivated by day 10 in *Ptf1a* cKO mice.

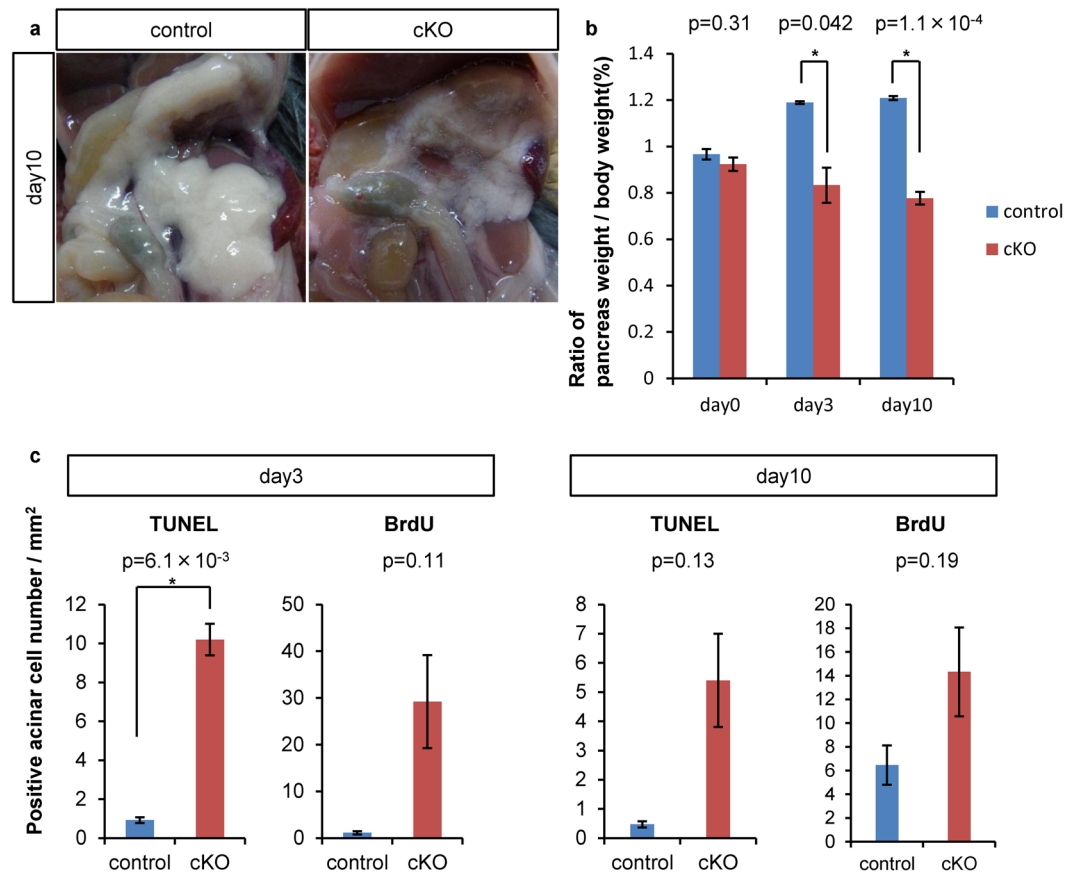


Figure 1. Acinar-specific *Ptf1a* deletion decreased pancreatic volume through activated apoptosis. (a) Representative pancreatic appearance of control and *Ptf1a* cKO mice on day 10. (b) Relative pancreatic weight per body weight. control, n = 3; *Ptf1a* cKO, n = 3. (c) The number of TUNEL or BrdU positive acinar cells per mm² on day 3 or 10. control, n = 3; *Ptf1a* cKO, n = 3. *P < 0.05.

***Xbp1* mRNA splicing was suppressed in *Ptf1a* cKO mice on day 3.** Next, we investigated the IRE1 pathway, which splices X-box binding protein 1 (*XBP1*) mRNA in response to ER stress in mammals¹⁶ (Fig. 5). Our RT-PCR analyses revealed a lower ratio of spliced *Xbp1* mRNA in *Ptf1a* cKO mice on day 3 but not on day 10, suggesting that the IRE1 pathway was suppressed on day 3 but recovered by day 10 in *Ptf1a* cKO mice.

ATF4 and CHOP were activated in *Ptf1a* cKO mice on day 3. Finally, we examined the PERK-eIF2 α -ATF4 pathway by ATF4 immunostaining. In control mice, no ATF4 signal in acinar cells was observed. On the other hand, in *Ptf1a* cKO mice, there was sporadic ATF4 expression predominantly in PTF1A-absent cells on day 3 and almost no ATF4 expression on day 10 (Fig. 6a). Thus, both the ATF6 pathway (Fig. 4) and the PERK-eIF2 α -ATF4 axis were upregulated on day 3 but returned to normal activation status by day 10 in *Ptf1a* cKO mice, which is consistent with our electron microscopy observations (Fig. 3). Furthermore, some cells on day 3 showed immunoreactivity for CHOP, a pro-apoptotic factor^{17,18}, but not on day 10 (Fig. 6b). CHOP immunoreactivity was observed in both ATF4(+) and ATF4(-) cells. Considering that CHOP is a downstream target of the ATF6 and PERK-eIF2 α -ATF4 pathways^{19,20}, ATF4(-)CHOP(+) cells may represent activation of the ATF6 pathway. Taken together, these findings suggest that acinar cell death in *Ptf1a* cKO mice is caused by excessive UPR. Intriguingly, we observed rare CHOP-PTF1A double positive cells in the mutants on day 3 (Fig. 6c), suggesting non-autonomous cell death in *Ptf1a*-preserved cells (Fig. 2c).

Discussion

Here we show that conditional *Ptf1a* loss in adult acinar cells causes ER stress and activates apoptosis pathways to decrease pancreatic size. It is known that the accumulation of unfolded or misfolded proteins in the ER causes ER stress^{13,14}. In response, cells escape from the stress status by activating the PERK-eIF2 α -ATF4, ATF6 and IRE1 pathways¹⁵. Each of these three pathways has a specific effect on the cell response to ER stress. PERK phosphorylates eIF2 α ²¹ to attenuate the translation of most genes except those that have a specific upper open reading frame such as ATF4²², thereby preventing additional stress acutely¹⁵. Cleaved ATF6 activates an ER chaperone to restore the protein folding machinery^{20,23}. IRE1 splices *Xbp1* mRNA to promote protein degradation²⁴ and thus decrease ER stress¹⁵. These mechanisms protect the cell from ER stress, but under excessive stress intensity and duration, prolonged expression of ATF4 and cleaved ATF6 upregulates the pro-apoptotic protein CHOP, which promotes cell death^{15,17-20}. In *Ptf1a* cKO mice, we confirmed activation of the PERK-eIF2 α -ATF4 and ATF6 pathways plus

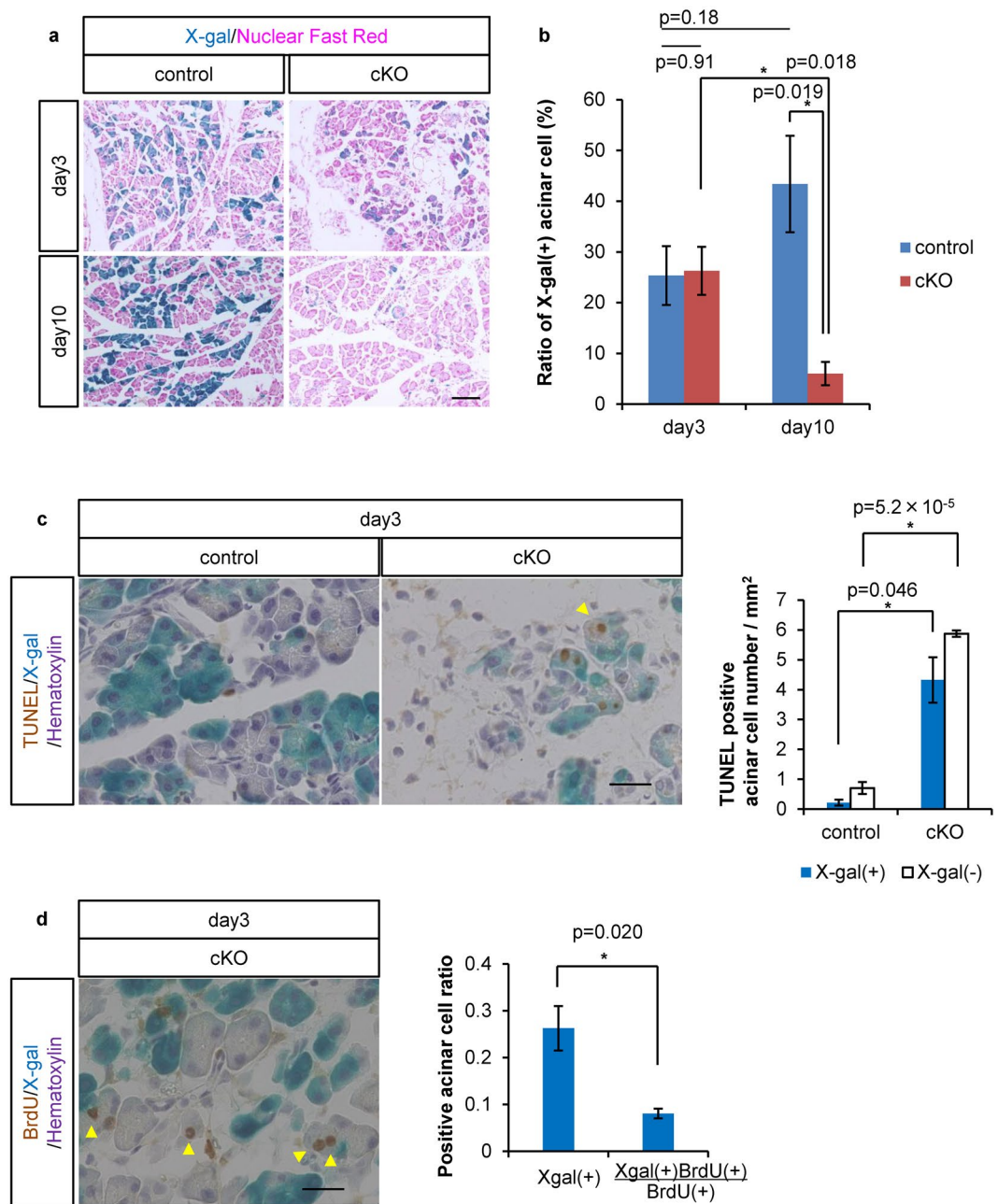


Figure 2. Lineage tracing revealed activated apoptosis and compensatory proliferation in *Ptf1a* cKO pancreata. (a) Representative figures of control and *Ptf1a* cKO mice on day 3 and day 10 stained by X-gal and Nuclear Fast Red. (b) The ratio of X-gal labeled acinar cells. control, $n = 3$; *Ptf1a* cKO, $n = 3$. (c) Representative figures of TUNEL staining with X-gal and hematoxylin staining, and the number of TUNEL(+) acinar cells per mm^2 on day 3. (d) Representative figure of BrdU staining with X-gal and hematoxylin staining, and the ratio of X-gal(+) BrdU(+) cells per total BrdU(+) cells compared with the ratio of X-gal(+) cells in *Ptf1a* cKO mice on day 3. Arrowheads indicate an X-gal(-)TUNEL(+) nucleus in (c) or X-gal(-)BrdU(+) nuclei in (d) in *Ptf1a* cKO mice. Scale bars = $100\ \mu\text{m}$ (a) or $25\ \mu\text{m}$ (c,d). * $P < 0.05$.

subsequent CHOP upregulation, and suppression of the IRE1 pathway. These findings suggest acinar cells in mutant mice are not in a cytoprotective state.

Unlike in our model, Krah *et al.* showed no difference in acinar cell death between control and *Ptf1a* cKO mice on day 14¹⁰, while Hoang *et al.* observed more apoptosis and UPR change in *Ptf1a* cKO mice than control¹¹. In addition, consistent with the autophagy they detected, they showed that *Xbp1* mRNA splicing was upregulated on days 6 and 14, indicating a cytoprotective response. On the other hand, consistent with the ER stress we detected, we showed different UPR on day 3, indicating an apoptotic response. We speculate that the phenotypic differences between ours and previous models might be explained by the original PTF1A dosage before the depletion. In our experiments, PTF1A dosage decreased from the homozygous-to-null status, whereas in previous models

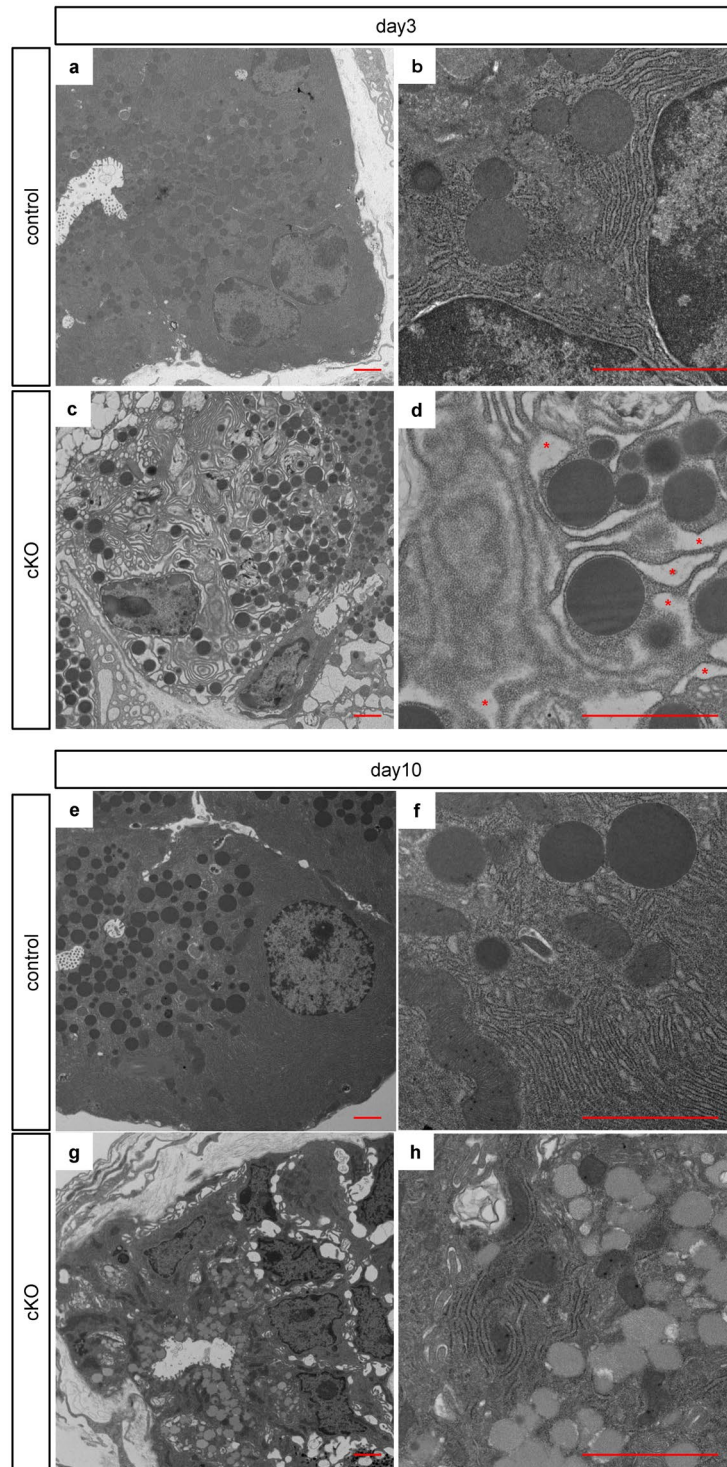


Figure 3. Activated endoplasmic reticulum stress in acinar cells of *Ptf1a* cKO mice. Representative findings of electron microscopy in control mice on day 3 (a) in *Ptf1a* cKO mice on day 3 (c) in control mice on day 10 (e) and in *Ptf1a* cKO mice on day 10 (g). (b,d,f,h) are magnified images of (a,c,e,g). Note the dilated ER lumen (indicated by red asterisks) in *Ptf1a* cKO mice on day 3 (d). Scale bars = 2 μ m.

the dosage decreased from the heterozygous-to-null status. Therefore, a more dynamic change in PTF1A expression should have occurred in our model. Presumably, adult acinar cells could not adapt to the rapid and massive decrease of PTF1A expression that caused severe ER stress.

At the same time, several observations were consistent with ours and previous reports. For example, we observed ADM in *Ptf1a* cKO mice. ADM cells may have escaped the apoptotic cell death machinery and survived by discarding their cell identity as acinar cells. Krahn *et al.* provided evidence that CD45(+) immune cells

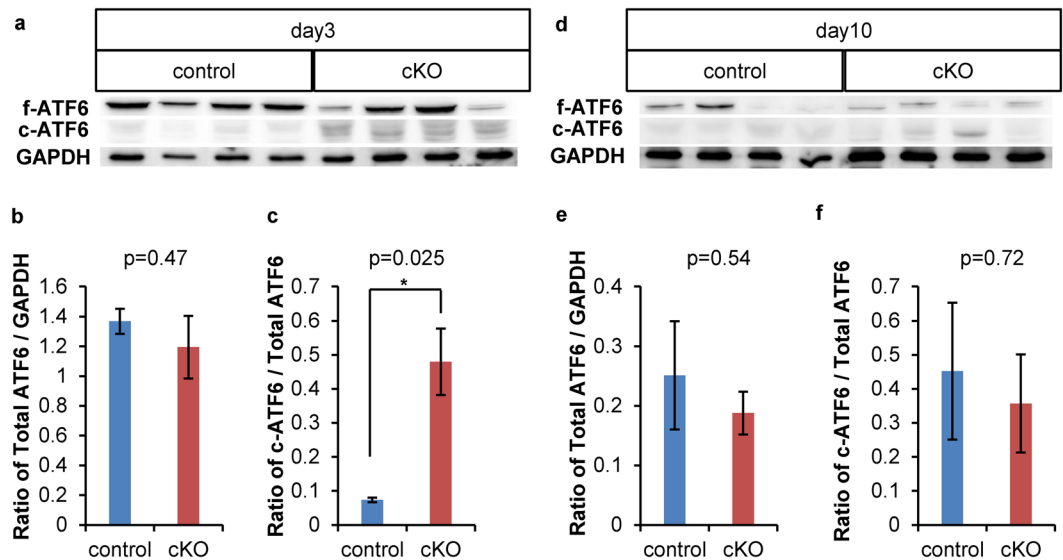


Figure 4. Cleavage of ATF6 was upregulated in *Ptf1a* cKO mice on day 3 but recovered by day 10. **(a)** Western blotting of control and *Ptf1a* cKO mice on day 3. **(b)** Comparison of the ratio of total ATF6/GAPDH expression in control and *Ptf1a* cKO mice on day 3. **(c)** Comparison of the ratio of cleaved ATF6/total ATF6 expression in control and *Ptf1a* cKO mice on day 3. **(d)** Western blotting of control and *Ptf1a* cKO mice on day 10. **(e)** Comparison of the ratio of total ATF6/GAPDH expression in control and *Ptf1a* cKO mice on day 10. **(f)** Comparison of the ratio of cleaved ATF6/total ATF6 expression in control and *Ptf1a* cKO mice on day 10. f-ATF6: full length ATF6, c-ATF6: cleaved ATF6. control, n = 4; *Ptf1a* cKO, n = 4. *P < 0.05. The original, unprocessed scans of the blots are shown in Supplementary Fig. S5.

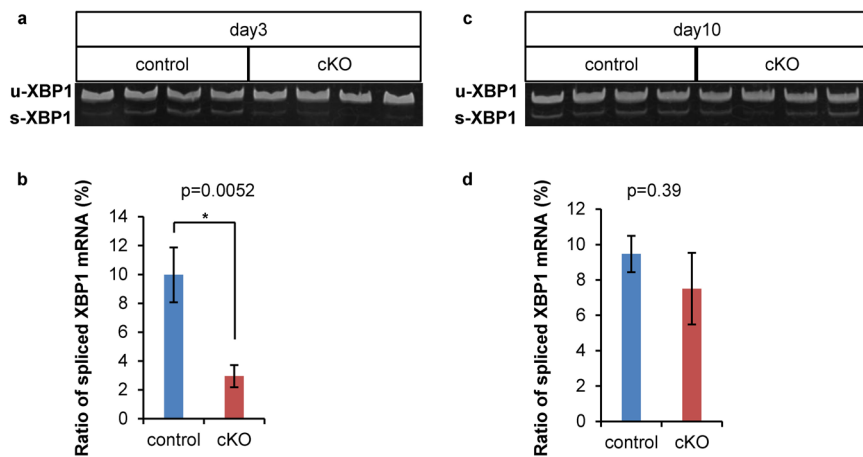


Figure 5. Splicing of *Xbp1* mRNA was suppressed in *Ptf1a* cKO mice on day 3 but recovered by day 10. **(a)** Representative electrophoresis of RT-PCR products of unspliced and spliced *Xbp1* mRNA on day 3. **(b)** Comparison of the percentage of spliced *Xbp1* mRNA on day 3 in control and *Ptf1a* cKO mice. control, n = 5; *Ptf1a* cKO, n = 6. **(c)** Representative electrophoresis of RT-PCR products of unspliced and spliced *Xbp1* mRNA on day 10. **(d)** Comparison of the percentage of spliced *Xbp1* mRNA on day 10 in control and *Ptf1a* cKO mice. control, n = 6; *Ptf1a* cKO, n = 5. *P < 0.05. The original, unprocessed scans of the gels are shown in Supplementary Fig. S6.

accumulate upon *Ptf1a* deletion and that caerulein-induced pancreatitis causes more ADM in *Ptf1a* cKO mice¹⁰. Considering that caerulein-induced pancreatitis itself reduces PTF1A expression²⁵ and causes ER stress²⁶ in acute phase, we propose there exists an interdependence among inflammation, ER stress and the maintenance of acinar cell identity or cell death, in which PTF1A expression plays a crucial role. In this study, we observed accelerated apoptosis and compensatory proliferation of the *Ptf1a*-preserved cells in the mutant pancreata. These observations indicate the competition between *Ptf1a*-deleted and -preserved cells, in which non-cell autonomous regulation plays a role. The precise mechanism including the identification of responsible signals warrants future investigation.

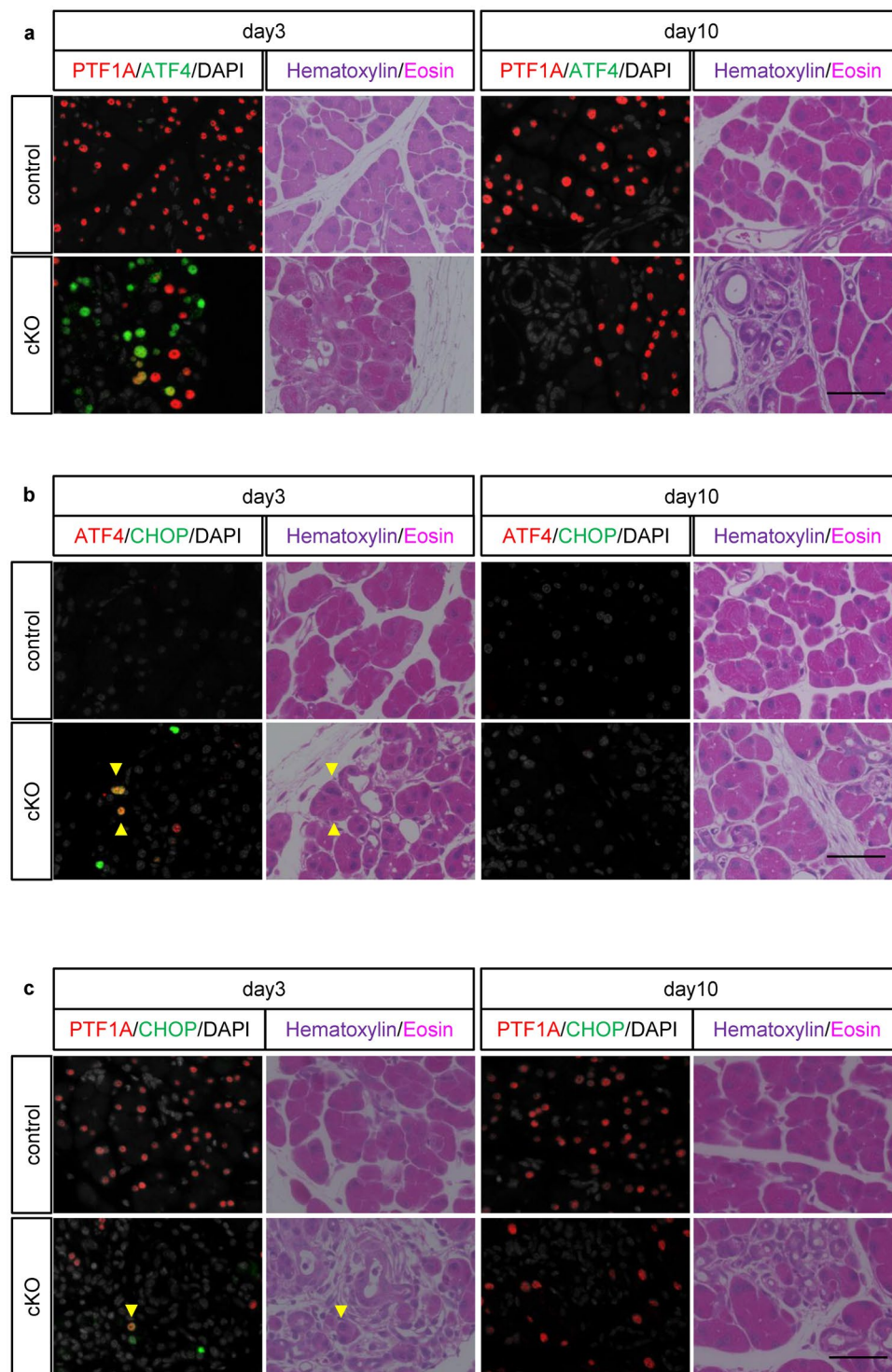


Figure 6. ATF4 and CHOP were upregulated in *Ptf1a* cKO mice on day 3 but recovered by day 10. Immunofluorescence of (a) PTF1A and ATF4 (b) ATF4 and CHOP, and (c) PTF1A and CHOP with hematoxylin-eosin staining on days 3 and 10. Arrowheads indicate CHOP and ATF4 double positive nuclei in (b) or a PTF1A and CHOP double positive nucleus in (c). Hematoxylin-eosin was stained on the same sections after immunofluorescence. Scale bars = 50 μ m.

In summary, we demonstrated that the homozygous-to-null reduction of *Ptf1a* triggered excessive UPR through activation of the ATF6 and PERK-eIF2 α -ATF4 pathways and suppression of the IRE1 pathway in adult acinar cells. Future studies are required to dissect how acinar cells initiate apoptosis or survive (for example, by changing their identity from acinar to duct-like) upon the rapid and dynamic reduction of PTF1A expression.

Methods

Mice. *Elastase-CreERTM*, *Rosa26R*, *Rosa26-RFP* and *Ptf1a^{flxed}* mice were previously described^{27–30}. By mating, we obtained *Elastase-CreERTM*; *Ptf1a^{flxed/flxed}*; *Rosa26R* or *Rosa26-RFP* mice (*Ptf1a* cKO mice) in which *Ptf1a*-deleted cells are detected as X-gal(+) or RFP(+) cells after tamoxifen injection. All animal experiments were performed in accordance with the Kyoto University guidelines for animal experiments and approved by the animal research committee of Kyoto University.

Drug injection. For lineage tracing, 8-week-old mice were injected once intraperitoneally with tamoxifen (T5648, Sigma-Aldrich, St. Louis, MO, USA) at 0.2 mg/g body weight. For BrdU staining, mice were injected intraperitoneally with BrdU (Merck Millipore, Billerica, MA, USA) at 2 mg 1 hour before euthanization.

Tissue preparation. All tissue preparations were performed as previously described³¹ with some modification. Briefly, for X-gal staining, ice-cold fixative solution (4% paraformaldehyde (PFA), 1% glutaraldehyde (GA)/PBS) was perfused into mice, and specimens were immersed into 4% PFA/PBS for 2 hours at 4 °C followed by 30% sucrose/PBS until equilibration and then embedded into O.C.T. compound (Sakura, Osaka, Japan). For raw RFP sections, the fixative solution perfused was 4% PFA/PBS, and specimens were immersed into the same solution for 4 hours at 4 °C followed by 30% sucrose/PBS until equilibration and then embedded into O.C.T. compound. For paraffin sections, the fixative solution perfused was 4% PFA/PBS, and specimens were immersed into the same solution overnight at 4 °C, then dehydrated in graded alcohol, immersed in Histo-Clear (National Diagnostics, Atlanta, GA, USA) and finally embedded into paraffin.

X-gal staining, immunohistochemistry, immunofluorescence and alcian blue staining. Frozen sections were cut into 4- μ m-thick slices. For X-gal staining, they were reacted at room temperature overnight as previously reported³¹ with some modifications. For TUNEL assays, DeadEnd Colorimetric Apoptosis Detection System (Promega Corporation, Madison, WI, USA) was used in accordance with the manufacturer's protocols. Paraffin sections were cut into 2- μ m-thick slices, deparaffinized and rehydrated. For either immunohistochemistry or immunofluorescence, the procedures from antigen retrieval to antibody reaction were done as previously reported³², however, heat induced epitope retrieval was omitted in the cases of raw RFP detection. The primary antibodies used are listed in Supplementary Table S1 and the secondary antibodies in Supplementary Table S2. The slices were treated with DAB Peroxidase Substrate (SK-4100, Vector Laboratories) for immunohistochemistry or with TSA Plus System (PerkinElmer, Waltham, MA, USA) and 4,6-diamidino-2-phenylindole (DAPI) for immunofluorescence. For alcian blue staining, sections were immersed into 3% acetic acid and then reacted with Alcian Blue Stain Solution pH 2.5 (Muto Pure Chemicals, Tokyo, Japan) for 20 minutes. Sections were counterstained by Nuclear Fast Red (Seracare, Milford, MA, USA), hematoxylin and/or eosin (Wako, Osaka, Japan), as previously reported³¹. Images were visualized using HS All-in-one Fluorescence Microscopy BZ-9000E (Keyence, Osaka, Japan).

Cell counting. For labeled cell assessment, we chose 30 fields (3 random views per section, 10 sections at equal intervals) at $\times 200$ magnification, counted X-gal positive and negative acinar cells (at least 20,000 cells) in each mouse and calculated the ratio. For PTF1A depletion assessment, we counted at least 700 RFP(+) cells from 30 or 50 fields (3 or 5 random views per section, 10 sections at equal intervals) in each mouse. For BrdU and TUNEL analyses, positive cells were counted in 50 fields (5 random views per section, 10 sections at equal intervals).

Alcian blue(+) area evaluation. 10 paraffin sections at equal intervals were stained by alcian blue, and whole images were taken. Whole pancreatic and alcian blue(+) areas were enclosed manually and quantified with BZ-H1M software (Keyence).

Electron microscopy. For tissue preparation, 4% PFA and 2% GA/PBS was perfused into mice. Specimens were cut into approximately 1 mm³ sections, immersed into the same solution overnight at 4 °C, and brought to Division of Electron Microscopic Study (DEMS), Center for Anatomical Studies, Graduate School of Medicine, Kyoto University. DEMS conducted the osmium tetroxide postfixation and the preparation of ultrathin sections with uranium staining. The sections were observed using a transmission electron microscope (Hitachi H-7650, Hitachi, Tokyo, Japan).

Western blotting. Whole pancreatic tissues were used. The procedures from lysate preparation to antibody reaction were reported previously³². The primary antibodies used are listed in Supplementary Table S3 and the secondary antibodies in Supplementary Table S4. Chemiluminescence was detected with Chemi-Lumi One Super (Nacal Tesque, Kyoto, Japan) and visualized with ImageQuant LAS 4000 (GE Healthcare, Chicago, IL, USA). The intensity of the bands was quantified with ImageQuant TL software (GE Healthcare), and the intensity ratio was calculated.

RNA isolation and data analysis. Total pancreatic RNA was extracted using RNeasy Mini Kit (Qiagen, Hilden, Germany) in accordance with the manufacturer's protocols. First strand cDNA synthesis was performed using ReverTra Ace qPCR RT Master Mix (Toyobo, Osaka, Japan). Measurement of the ratio of spliced to total *Xbp1* mRNA was performed by RT-PCR using forward primer 5'-AGTTAAGAACACGCTTGGGAAT-3' and reverse primer 5'-AAGATGTTCTGGGGAGGTGAC-3'. PCR products were 172 bp for unspliced *Xbp1* mRNA and 146 bp for spliced *Xbp1* mRNA. The products were electrophoresed in 10% acrylamide gel in TBE, stained with ethidium bromide, and visualized with ChemiDoc XRS + system (Bio-Rad Laboratories, Hercules, CA, USA). The intensity of the bands was quantified with Image Lab Software (Bio-Rad Laboratories), and the intensity ratio was calculated.

Statistical analysis. All values are shown as means \pm s.e.m. All error bars represent s.e.m. All indices were analyzed using an unpaired t test (two-tailed). $P < 0.05$ was considered significant.

References

1. Takahashi, K. & Yamanaka, S. Induction of pluripotent stem cells from mouse embryonic and adult fibroblast cultures by defined factors. *Cell* **126**, 663–76 (2006).
2. Takahashi, K. *et al.* Induction of pluripotent stem cells from adult human fibroblasts by defined factors. *Cell* **131**, 861–72 (2007).
3. Davis, R. L., Weintraub, H. & Lassar, A. B. Expression of a single transfected cDNA converts fibroblasts to myoblasts. *Cell* **51**, 987–1000 (1987).
4. Sekiya, S. & Suzuki, A. Direct conversion of mouse fibroblasts to hepatocyte-like cells by defined factors. *Nature* **475**, 390–3 (2011).
5. Krapp, A. *et al.* The bHLH protein PTF1-p48 is essential for the formation of the exocrine and the correct spatial organization of the endocrine pancreas. *Genes Dev* **12**, 3752–63 (1998).
6. Kawaguchi, Y. *et al.* The role of the transcriptional regulator Ptf1a in converting intestinal to pancreatic progenitors. *Nat Genet* **32**, 128–34 (2002).
7. Krapp, A. *et al.* The p48 DNA-binding subunit of transcription factor PTF1 is a new exocrine pancreas-specific basic helix-loop-helix protein. *EMBO J* **15**, 4317–29 (1996).
8. Masui, T. *et al.* Transcriptional autoregulation controls pancreatic Ptf1a expression during development and adulthood. *Mol Cell Biol* **28**, 5458–68 (2008).
9. Fukuda, A. *et al.* Reduction of Ptf1a gene dosage causes pancreatic hypoplasia and diabetes in mice. *Diabetes* **57**, 2421–31 (2008).
10. Krah, N.M. *et al.* The acinar differentiation determinant PTF1A inhibits initiation of pancreatic ductal adenocarcinoma. *Elife* **4** (2015).
11. Hoang, C. Q. *et al.* Transcriptional Maintenance of Pancreatic Acinar Identity, Differentiation, and Homeostasis by PTF1A. *Mol Cell Biol* **36**, 3033–3047 (2016).
12. Rodolosse, A. *et al.* PTF1 α /p48 transcription factor couples proliferation and differentiation in the exocrine pancreas [corrected]. *Gastroenterology* **127**, 937–49 (2004).
13. Alanen, A., Pira, U., Lassila, O., Roth, J. & Franklin, R. M. Mott cells are plasma cells defective in immunoglobulin secretion. *Eur J Immunol* **15**, 235–42 (1985).
14. Pavelka, M. & Roth, J. Third edition. *Functional Ultrastructure: Atlas of Tissue Biology and Pathology*, 48–49 (Springer-Verlag Vienna, 2015).
15. Waldron, R. T., Pandol, S., Lugea, A. & Groblewski, G. Endoplasmic reticulum stress and the unfolded protein response in exocrine pancreas physiology and pancreatitis. October 16, 2015 edn (Pancreapedia: Exocrine Pancreas Knowledge Base, <https://doi.org/10.3998/panc.2015.41>, 2015).
16. Yoshida, H., Matsui, T., Yamamoto, A., Okada, T. & Mori, K. XBP1 mRNA is induced by ATF6 and spliced by IRE1 in response to ER stress to produce a highly active transcription factor. *Cell* **107**, 881–91 (2001).
17. Friedman, A. D. GADD153/CHOP, a DNA damage-inducible protein, reduced CAAT/enhancer binding protein activities and increased apoptosis in 32D c13 myeloid cells. *Cancer Res* **56**, 3250–6 (1996).
18. Cai, Y. *et al.* TRAM1 protects AR42J cells from caerulein-induced acute pancreatitis through ER stress-apoptosis pathway. *In Vitro Cell Dev Biol Anim* **52**, 530–6 (2016).
19. Fawcett, T. W., Martindale, J. L., Guyton, K. Z., Hai, T. & Holbrook, N. J. Complexes containing activating transcription factor (ATF)/cAMP-responsive-element-binding protein (CREB) interact with the CCAAT/enhancer-binding protein (C/EBP)-ATF composite site to regulate Gadd153 expression during the stress response. *Biochem J* **339**(Pt 1), 135–41 (1999).
20. Yoshida, H. *et al.* ATF6 activated by proteolysis binds in the presence of NF-Y (CBF) directly to the cis-acting element responsible for the mammalian unfolded protein response. *Mol Cell Biol* **20**, 6755–67 (2000).
21. Harding, H. P., Zhang, Y. & Ron, D. Protein translation and folding are coupled by an endoplasmic-reticulum-resident kinase. *Nature* **397**, 271–4 (1999).
22. Harding, H. P. *et al.* Regulated translation initiation controls stress-induced gene expression in mammalian cells. *Mol Cell* **6**, 1099–108 (2000).
23. Haze, K., Yoshida, H., Yanagi, H., Yura, T. & Mori, K. Mammalian transcription factor ATF6 is synthesized as a transmembrane protein and activated by proteolysis in response to endoplasmic reticulum stress. *Mol Biol Cell* **10**, 3787–99 (1999).
24. Yoshida, H. *et al.* A time-dependent phase shift in the mammalian unfolded protein response. *Dev Cell* **4**, 265–71 (2003).
25. Molero, X. *et al.* Pancreas transcription factor 1 α expression is regulated in pancreatitis. *Eur J Clin Invest* **37**, 791–801 (2007).
26. Seyhun, E. *et al.* Tauroursodeoxycholic acid reduces endoplasmic reticulum stress, acinar cell damage, and systemic inflammation in acute pancreatitis. *Am J Physiol Gastrointest Liver Physiol* **301**, G773–82 (2011).
27. Soriano, P. Generalized lacZ expression with the ROSA26 Cre reporter strain. *Nat Genet* **21**, 70–1 (1999).
28. Stanger, B. Z. *et al.* Pten constrains centroacinar cell expansion and malignant transformation in the pancreas. *Cancer Cell* **8**, 185–95 (2005).
29. Luche, H., Weber, O., Nageswara Rao, T., Blum, C. & Fehling, H. J. Faithful activation of an extra-bright red fluorescent protein in “knock-in” Cre-reporter mice ideally suited for lineage tracing studies. *Eur J Immunol* **37**, 43–53 (2007).
30. Fujiyama, T. *et al.* Forebrain Ptf1a Is Required for Sexual Differentiation of the Brain. *Cell Rep* **24**, 79–94 (2018).
31. Furuyama, K. *et al.* Continuous cell supply from a Sox9-expressing progenitor zone in adult liver, exocrine pancreas and intestine. *Nat Genet* **43**, 34–41 (2011).
32. Goto, T. *et al.* Liver-specific Prox1 inactivation causes hepatic injury and glucose intolerance in mice. *FEBS Lett* **591**, 624–635 (2017).

Acknowledgements

This work was supported by the Funding Program for Next Generation World-Leading Researchers, Japan Society for the Promotion of Science [grant number LS063]. We thank P. Karagiannis for proofreading, and the staff of the Institute of Laboratory Animals at Graduate School of Medicine, Kyoto University, for animal care. The electron microscopy study was supported by Keiko Okamoto-Furuta and Haruyasu Kohda (Division of Electron Microscopic Study, Center for Anatomical Studies, Graduate School of Medicine, Kyoto University).

Author Contributions

Y.K. and M.S. designed the study, analyzed the data and prepared the manuscript. M.S. performed the experiments. Y.D. generated the mice. T.F. and Mi.H. generated the *Ptf1a^{floxex}* mice. Mi.H. provided the anti-PTF1A antibody. K.F., Ma.H., S.H., Y.A., K.T., T.G., K.H. and T.M. gave technical support and discussion. S.U. and Y.K. supervised the project.

Additional Information

Supplementary information accompanies this paper at <https://doi.org/10.1038/s41598-018-34093-4>.

Competing Interests: The authors declare no competing interests.

Publisher's note: Springer Nature remains neutral with regard to jurisdictional claims in published maps and institutional affiliations.



Open Access This article is licensed under a Creative Commons Attribution 4.0 International License, which permits use, sharing, adaptation, distribution and reproduction in any medium or format, as long as you give appropriate credit to the original author(s) and the source, provide a link to the Creative Commons license, and indicate if changes were made. The images or other third party material in this article are included in the article's Creative Commons license, unless indicated otherwise in a credit line to the material. If material is not included in the article's Creative Commons license and your intended use is not permitted by statutory regulation or exceeds the permitted use, you will need to obtain permission directly from the copyright holder. To view a copy of this license, visit <http://creativecommons.org/licenses/by/4.0/>.

© The Author(s) 2018